# Estimate Aβ-PET Pattern from fMRI Data based on Deep Learning

Siqing Yuan, School of Biomedical Engineering, ShanghaiTech University, Shanghai, China

***ABSTRACT*—Alzheimer's disease (AD) is a progressive and irreversibly neurodegenerative disease characterized by a stealthy onset. In the realm of neuroimaging, the detection of aberrant amyloid-beta (Aβ) deposition patterns via positron emission tomography (PET) is heralded as the gold standard for the early diagnosis of AD. However, the use of radioactive tracers in PET scans is not conducive to elderly individuals with declining physical function. This study introduces an innovative integrated framework leveraging graph convolutional networks to predict individual Aβ-PET deposition patterns by harnessing multi-level functional connectivity (FC) data derived from resting-state functional magnetic resonance imaging (rs-fMRI). The methodology was rigorously evaluated on the Open Access Series of Imaging Studies (OASIS) dataset, where it demonstrated satisfactory accuracy and robustness in the prediction of standardized uptake value ratios (SUVR) across global cerebral regions.**

***INDEX TERMS*—Functional connectivity, High-order functional connectivity, Aβ-PET, Graph convolutional networks**

## INTRODUCTION

Alzheimer's disease (AD) is a neurodegenerative disorder characterized by insidious onset and progressive course [1]. Clinically, AD manifests as comprehensive dementia with symptoms including memory impairment, aphasia, apraxia, agnosia, visuo-spatial skill deficits, executive dysfunction, and alterations in personality and behavior [2]. Given the incompletely understood pathogenesis of AD and the challenges in preemptive prevention, early diagnosis is of paramount importance.

Biological markers commonly associated with AD include beta-amyloid (Aβ) and tau proteins [3]. Among these, tau protein quantification typically requires cerebrospinal fluid samples obtained via lumbar puncture, a procedure less accessible than methods for detecting Aβ. Abnormal Aβ deposition patterns identified through positron emission tomography (Aβ-PET pattern) are regarded as the imaging gold standard for early diagnosis of AD before the onset of cognitive symptoms [4], [5]. Quantitative representation of Aβ patterns is often achieved through thermographic mapping of the standardized uptake value ratio (SUVR) of Aβ protein across various cerebral regions, assisting physicians in diagnosis through the spatial distribution of these patterns. Furthermore, the distribution of Aβ protein deposition within brain regions is also valuable for assessing the therapeutic effects of targeted drug delivery, underscoring its significance for scientific research.

However, the applicability of PET scans is limited by factors such as renal function decline and cardio-vascular health issues prevalent in the elderly. Thus, various non-invasive MRI techniques have been pursued for the early diagnosis of AD [6], [7]. Studies have demonstrated a significant correlation between functional connectivity maps generated by resting-state functional magnetic resonance imaging (rs-fMRI) and Aβ-PET patterns [8], [9]. Therefore, if the association between the two can be accurately characterized, it is conceivable to obtain Aβ patterns through rs-fMRI. The increasing application of Graph Convolutional Net-works (GCNs) in neuro-imaging, coupled with their demonstrated efficacy in extracting information pertinent to Alzheimer's disease (AD) from functional connectivity maps [10], provides strong grounds to posit

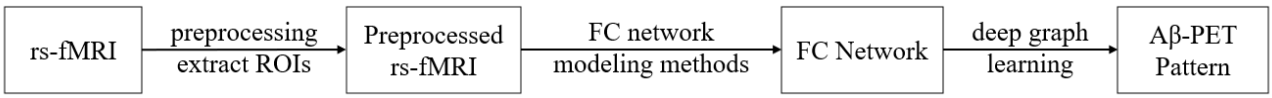


Fig. 1 Pipeline for Predicting Aβ-PET Patterns from rs-fMRI Data

that GCNs can make a significant contribution to elucidating this association.

Moreover, research from Stanford University has indicated that the functional connectivity derived from rs-fMRI may exhibit dynamic variations over time scales from seconds to minutes, and measuring this variability could be of significant value [11]. A novel method for extracting high-order functional connectivity (HOFC) correlations characterizes how low-order FC between different brain regions interact and has been applied to the classification tasks in mild cognitive impairment (MCI) [12]. Therefore, our study incurporates both the derived low-order FC networks and dynamic high-order functional connectivity (dHOFC) from rs-fMRI to capture a richer spectrum of cerebral information, thereby generating model outputs that more accurately reflect the patterns in Aβ-PET imaging.

## METHOD

### Pipeline

In this study, we aim to employ resting-state functional magnetic resonance imaging (rs-fMRI) data as input to predict the corresponding individual's amyloid-beta positron emission tomography (Aβ-PET) pattern. The workflow is illustrated in Fig. 1. Initially, the raw data undergo preprocessing and extraction of regions of interest (ROIs); subsequently, we employ functional connectivity (FC) modeling techniques to construct both lower-order and higher-order FC networks from the preprocessed fMRI data, integrating multi-level information into a graph network model; ultimately, we harness the capabilities of graph convolutional networks (GCNs) to extract features from the multi-level FC networks, thereby predicting the final Aβ-PET pattern.

### Dataset

The dataset employed for the construction and validation of our method was sourced from the Open Access Series of Imaging Studies 3 (OASIS-3) [13], encompassing T1-weighted structural MRI (sMRI), amyloid-beta positron emission tomography (Aβ-PET), and resting-state functional MRI (rs-fMRI) scans. Data were provided by a cohort of 228 participants, yielding a total of 258 datasets (100 from male participants and 158 from female participants), with ages ranging from 42 to 89 years.

Table 1 summarizes the parameters utilized for the acquisition of input and label data. Additionally, PET imaging was conducted using the radiotracer [11C]-Pittsburgh compound B (PiB), and a repetition time (TR) of 2.2 seconds was set for the rs-fMRI scans.

TABLE I Acquisition Parameters for PET and rs-fMRI

| | Instrument | Time points | Spatial resolution |
|---|---|---|---|
| PET | Siemens Biograph 40 PET/CT | 26 | 2.3×2.3×2 $mm^3$ |
| rs-fMRI | Siemens Trio Tim 3.0T MRI / Siemens BioGraph mMR 3.0T PET-MR | 164 | 4×4×4 $mm^3$ |

### Step1. Preprocessing

The Aβ-PET standardized uptake value ratio (SUVR) data derived from the preprocessed PET images served as the labels for both training and testing within the overarching methodological framework. Initially, the PET images were subjected to preprocessing using the PET Unified Pipeline (PUP) [14]. Partial volume correction based on the regional spread function was employed to adjust the SUVR, which is calculated by dividing the standard uptake value (SUV) of each voxel by the mean cerebellar SUV. Subsequently, the Desikan-

Killiany (DK) atlas [15], available within the FreeSurfer software suite, was applied to segment the entire PET images for each individual. This segmentation yielded an average SUVR for 166 regions of interest (ROIs), encompassing both gray and white matter.

For the rs-fMRI input data, preprocessing was conducted using the BRANT fMRI toolkit [16]. The preprocessing pipeline (Fig. 2) included the exclusion of the first five time points as dummy scans and head motion correction for displacements less than 3mm or rotations below 3 degrees. The resampled fMRI data were set to a resolution of 3×3×3 $mm^3$, and spatial smoothing was performed using a 6mm full-width at half-maximum (FWHM) Gaussian kernel. Bandpass filtering was implemented to retain frequencies within the 0.01-0.08Hz range. Following this, fMRI signals for 600 ROIs were extracted from the fMRI volumes based on the Schaefer 2018 atlas, which were then utilized to construct the subsequent multi-level FC networks.

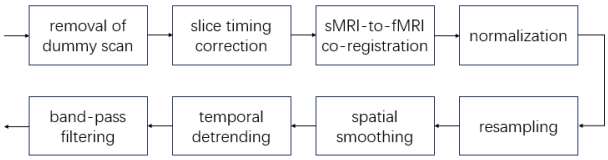


Fig. 2 Resting-State fMRI Data Preprocessing Pipeline

**Step2. Multi-level FC Network Construction**

To enhance the accuracy of predicting amyloid-beta positron emission tomography (Aβ-PET) deposition patterns, we employed resting-state functional magnetic resonance imaging (rs-fMRI) to construct functional connectivity (FC) networks at two hierarchical levels: lower-order and higher-order. These multi-level FC networks supply distinct tiers of functional organization information essential for subsequent graph convolutional network analysis, offering a superior advantage in the early detection of Alzheimer's Disease (AD) compared to single-layer FC analysis [12]. The lower-order FC network is predicated on traditional Pearson correlation (PC-based) brain networks, reflecting the temporal synchrony of blood-oxygen-level-dependent (BOLD) signals across various cerebral regions throughout the entire time series (488 seconds). Within the 600 extracted regions of interest (ROIs), we computed pairwise Pearson correlations to generate a static, node-based 600×600 network matrix.

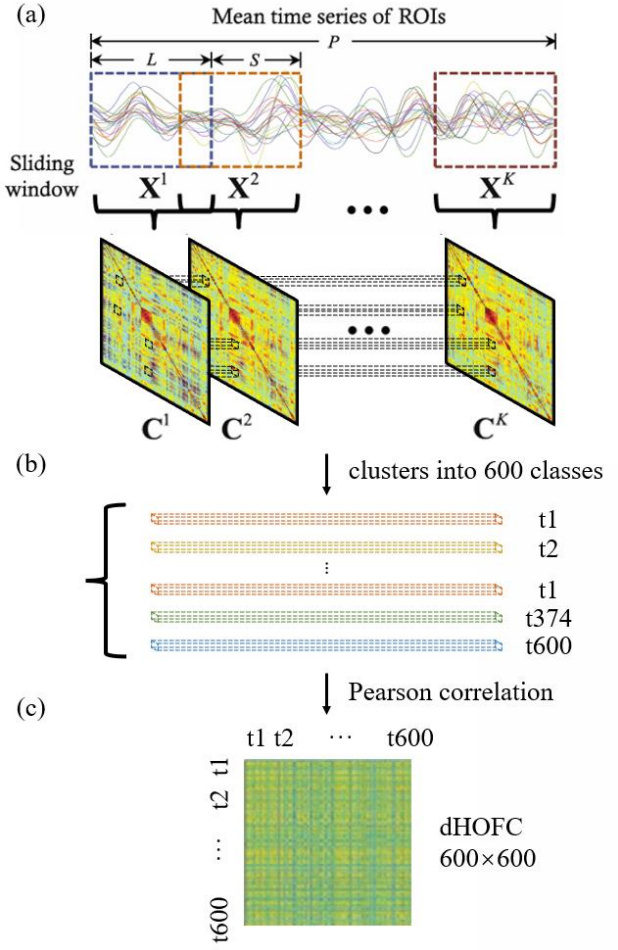


Fig. 3 Framework for construction of dynamic high-order FC network. (a) The total duration of the time series is 488 seconds, with a sliding window length of 66 seconds and a stride of 2.2 seconds, resulting in k=192 overlapping windows and corresponding lower-order FC graphs. (b) The formation of k-dimensional vectors, totaling ( 600×600×1/2-600 ), represents the temporal correlation series between ROI pairs. Clustering is performed using the k-means algorithm, with t1 denoting the classification of a k-dimensional correlation series into the first cluster. (c) The resulting dHOFC network is a 600×600 matrix.

Dynamic higher-order functional connectivity (dHOFC) encapsulates the dynamic temporal synchrony of FC among multiple ROI sets [11]. Conventionally, the generation of lower-order FC networks presupposes invariant functional connectivity during the entire

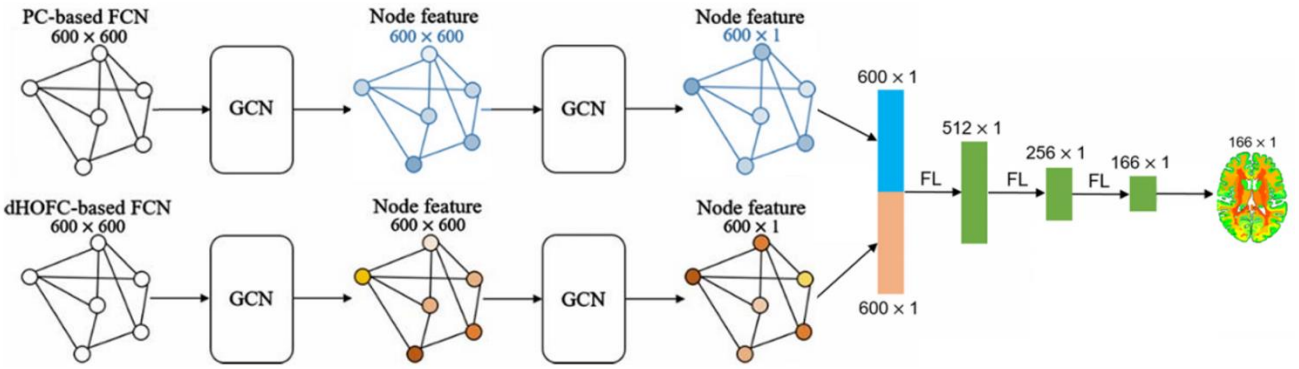


Fig. 4 The two-branch GCN network architecture for jointly PC- (the upper branch) and dHOFC- (the lower branch) based FC learning for individual Aβ-PET pattern predictions.

imaging time frame under resting-state conditions, thereby failing to portray fluctuations at finer temporal scales. To address this, we harnessed the BrainNetClass toolkit to compute dynamic higher-order FC through a sliding window technique [17].

Fig. 3 illustrates the schematic of the dynamic higher-order functional connectivity (dHOFC) network construction process. Initially, k shorter, overlapping sub-time series were derived from the complete rs-fMRI time series via sliding windows. Subsequently, for each sub-time series, we constructed a PC-based FC network of 600 ROIs (yielding k 600×600 matrices) to represent the short-term correlations between cerebral regions. These short-term PC-based FC networks were then stacked, forming a volumetric network matrix. Elements at identical positions across all PC-based FC networks were amalgamated into k-dimensional vectors. Owing to the symmetry of the network, a total of (600×600×1/2-600) distinct k-dimensional vectors were obtained, corresponding to the correlated time series of ROI pairs. To mitigate computational demands, we applied the k-means clustering algorithm to categorize all k-dimensional vectors into 600 clusters. Each cluster's mean temporal series was utilized as a new vertex, and pairwise Pearson correlation coefficients between these new vertices were computed. The resultant dHOFC (600×600) is a network predicated on edge-based connectivity.

**Step3. Integrated Network Architecture**

In the construction of our integrated learning network architecture, we employ one of the most effective graph learning algorithms, the Graph Convolutional Network (GCN) (Fig. 4). The inputs to this network comprise both lower-level and higher-level Functional Connectivity (FC) networks. For the lower-level FC network, we define the graph's nodal features using the one-hot encoding of the BOLD signals from 600 Regions of Interest (ROIs), and the graph's topological features are delineated by the FC among each pair of ROIs. Thus, the functional connectivity (FC) network is represented as a graph. To preserve the connectivity information, we refrain from binarizing the FC. Subsequently, we apply a two-layer graph convolution to this graph, aggregating information from adjacent nodes to extract the corresponding topological features, resulting in a novel nodal representation.

Similarly, for the higher-level dHOFC network, the nodal features are characterized by 600 correlated time series, and the graph's topological features are determined by the FC among these time series, forming a weighted graph topology. Two-layer graph convolution is then utilized to iteratively extract both topological and nodal features, yielding a more profound graph representation.

These processes constitute two branches of our GCN-based approach, each learning different levels of brain functional connectivity information. The subsequent step involves global average pooling of the advanced abstract nodal feature graphs obtained from both branches. The pooled features are then aggregated, enabling the simultaneous representation of both lower-

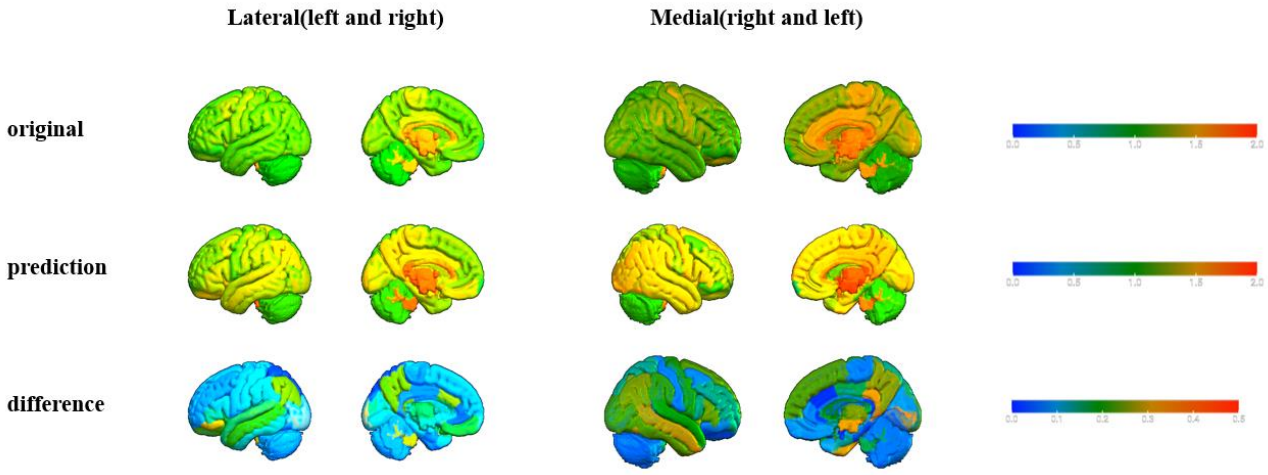


Fig. 5 Representative sample of Aβ-PET patterns showing the ground truth, predicted values, and their differences

level and higher-level brain features within a single vector. These dual forms of information are complementary. The features are propagated through three fully connected layers (with the final layer dimensioned at 166×1), ultimately mapping onto 166 ROIs as predefined by the Desikan-Killiany atlas, to produce the predicted Aβ-PET Standardized Uptake Value Ratio (SUVR) maps.

### Model Evaluation Using Five-Fold Cross-Validation

We assessed our model's performance using five-fold cross-validation, with the Mean Squared Error (MSE) as the loss function. Performance metrics were based on error and correlation between actual and predicted values. The data was randomly divided into five equal subsets. In each fold, four subsets formed the training set and the fifth served as the test set. This procedure was repeated five times to ensure each subset was used as a test set once. To evaluate the model's consistency, we conducted the five-fold cross-validation 30 times.

## RESULTS

Evaluation of our method via five-fold cross-validation yielded mean square error (MSE) and correlation metrics for the prediction of Aβ-PET patterns from rs-fMRI data. A comprehensive summary of the MSE and correlation coefficient distributions across all samples is presented in Fig. 6. The data indicate an average MSE of 0.048 and a mean correlation coefficient of 0.796 for the sample predictions relative to the ground truth. Except for two outliers, the MSE values for all samples were below 0.3, and correlation coefficients were consistently above 0.3.

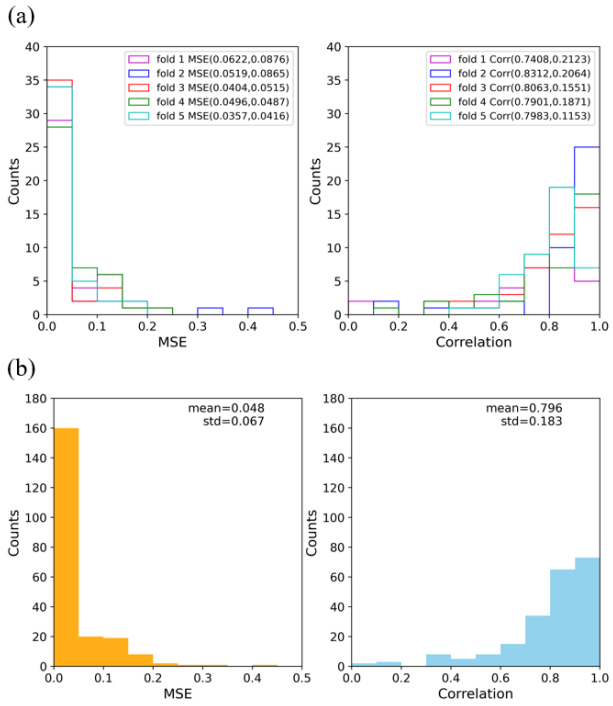


Fig. 6 (a) Depicts the Mean Square Error (MSE) and correlation coefficients for each fold of the test set. (b) Illustrates the distribution of MSE and correlation coefficients across all samples.

A representative sample was selected for detailed analysis, with the SUVR values for 166 ROIs (including actual, predicted, and residuals) within the Aβ-PET pattern visualized in a brain map (Fig. 5). The MSE was

generally below 0.3 across different ROIs.

Moreover, to evaluate the model's stability, parameters were randomly initialized, and sample subsets were randomly partitioned for 30 iterations of five-fold cross-validation. The distribution of MSE and correlation coefficients for each iteration is presented in Fig. 7. The average MSE remained stable between 0.06 and 0.08, with correlations around 0.8, demonstrating that our model can predict Aβ-PET patterns from rs-fMRI data with high accuracy and stability.

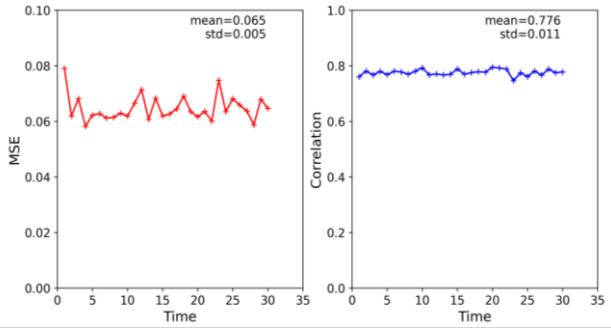


Fig. 7 Average MSE and correlation coefficients from 30 runs of five-fold cross-validation.

## DISCUSSION

In this study, we have introduced a novel algorithmic model capable of generating Aβ-PET pattern maps from individual rs-fMRI data, thereby circumventing the numerous limitations associated with PET scanning. The experimental results affirm the efficacy and stability of our proposed algorithm. This advancement holds the potential for aiding in the diagnosis of Alzheimer's Disease (AD) and propelling further research in the field.

Our methodology was applied to the OASIS dataset, which is characterized by relatively low spatial resolution, a factor that could potentially constrain the performance of our algorithm. Moreover, the generalizability of our model has not been extensively validated. In future research endeavors, we aim to deploy our model across a broader array of datasets to ascertain its applicability to other data cohorts. With further validation of our method's capabilities and robustness, this algorithm could provide diagnostic recommendations in settings where experienced clinicians are scarce or serve as a tool for large-scale screening of AD risk.

## REFERENCE

[1] Zvěřová, Martina. "Clinical aspects of Alzheimer's disease." Clinical biochemistry 72 (2019): 3-6.

[2] Karantzoulis, Stella, and James E. Galvin. "Distinguishing Alzheimer's disease from other major forms of dementia." Expert review of neurotherapeutics 11, no. 11 (2011): 1579-1591.

[3] Frankfort, Suzanne V., Linda R. Tulner, Jos PCM van Campen, Marcel M. Verbeek, Rene WMM Jansen, and Jos H. Beijnen. "Amyloid beta protein and tau in cerebrospinal fluid and plasma as biomarkers for dementia: a review of recent literature." Current clinical pharmacology 3, no. 2 (2008): 123-131.

[4] A. Nordberg, J. O. Rinne, A. Kadir, and B. Långström, "The use of PET in Alzheimer disease", Nat. Rev. Neurol., vol. 6, no. 2, pp. 78-87, 2010.

[5] C. R. Jack, D. A. Bennett, K. Blennow, M. C. Carrillo, B. Dunn, S. B. Haeberlein, et al., "NIA-AA Research Framework: Toward a biological definition of Alzheimer's disease", Alzheimers Dement., vol. 14, no. 4, pp. 535-562, 2018.

[6] M. Liu, D. Zhang, E. Adeli, and D. Shen, "Inherent Structure-Based Multiview Learning With Multi-template Feature Representation for Alzheimer's Disease Diagnosis", IEEE Trans. Biomed. Eng., vol. 63, no. 7, pp. 1473-1482, 2016.

[7] M. Liu, D. Zhang, and D. Shen, "Hierarchical fusion of features and classifier decisions for Alzheimer's disease diagnosis", Hum. Brain Mapp., vol. 35, no. 4, pp. 1305-1319, 2014.

[8] J. A. Elman, C. M. Madison, S. L. Baker, J. W. Vogel, S. M. Marks, S. Crowley, et al., "Effects of Beta-Amyloid on Resting State Functional Connectivity Within and Between Networks Reflect Known Patterns of Regional Vulnerability", Cereb. Cortex, vol. 26, no. 2, pp. 695-707, 2016.

[9] M. Yu, O. Sporns, and A. J. Saykin, "The human connectome in Alzheimer disease — relationship to biomarkers and genetics", Nat. Rev. Neurol., vol. 17, no. 9, pp. 545-563, 2021.

[10] C. Li, M. Liu, J. Xia, L. Mei, Q. Yang, F. Shi, et al., “Predicting Brain Amyloid-β PET Grades with Graph Convolutional Networks Based on Functional MRI and Multi-Level Functional Connectivity”, J. Alzheimers Dis., vol. 86, no. 4, pp. 1679-1693, 2022.
[11] Chang, Catie, and Gary H. Glover. "Time–frequency dynamics of resting-state brain connectivity measured with fMRI." Neuroimage 50, no. 1 (2010): 81-98.
[12] Wee, Chong-Yaw, Sen Yang, Pew-Thian Yap, Dinggang Shen, and Alzheimer’s Disease Neuroimaging Initiative. "Sparse temporally dynamic resting-state functional connectivity networks for early MCI identification." Brain imaging and behavior 10 (2016): 342-356.
[13] P. J. LaMontagne, T. L. S. Benzinger, J. C. Morris, S. Keefe, R. Hornbeck, C. Xiong, et al., “OASIS-3: Longitudinal Neuroimaging, Clinical, and Cognitive Dataset for Normal Aging and Alzheimer Disease”, 2019, medRxiv:2019.12.13.19014902.
[14] Y. Su, T. M. Blazey, A. Z. Snyder, M. E. Raichle, D. S. Marcus, B. M. Ances, et al., “Partial volume correction in quantitative amyloid imaging”, Neuroimage, vol. 107, pp. 55-64, 2015.
[15] R. S. Desikan, F. Ségonne, B. Fischl, B. T. Quinn, B. C. Dickerson, D. Blacker, et al., “An automated labeling system for subdividing the human cerebral cortex on MRI scans into gyral based regions of interest”, Neuroimage, vol. 31, no. 3, pp. 968-980, 2006.
[16] K. Xu, Y. Liu, Y. Zhan, J. Ren, and T. Jiang, “BRANT: A Versatile and Extendable Resting-State fMRI Toolkit”, Front. Neuroinform., vol. 12, pp. 52, 2018.
[17] Z. Zhou, X. Chen, Y. Zhang, D. Hu, L. Qiao, R. Yu, et al., “A toolbox for brain network construction and classification (BrainNetClass)”, Hum. Brain Mapp., vol. 41, no. 10, pp. 2808-2826, 2020.